Supplement of Atmos. Chem. Phys., 26, 9907–9927, 2026
https://doi.org/10.5194/acp-26-9907-2026-supplement

Atmospheric Chemistry and Physics
Open Access
EGU

Supplement of

Aerosol scavenging in DC3 and SEAC^{4}RS deep convective storms

Mary C. Barth et al.

Correspondence to: Mary C. Barth (barthm@ucar.edu)

S1. Methodology for determining passive trace gases used for the entrainment rate calculation

The entrainment rates were originally determined by previous work (Barth et al., 2016; Fried et al., 2016; Cuchiara et al., 2020; Cuchiara et al., 2023) where more details can be found. Here, we present the logic in choosing trace gases and list the trace gases used in the entrainment rate calculations as well as the entrainment rates determined from each trace gas for each storm case.

In choosing insoluble, passive trace gases for determining the entrainment rate in a storm, a few criteria are imposed. Insoluble trace gases generally have an effective Henry's Law constant of 1 M atm^{-1} or less and include trace gases like CO, O_3, NO, NO_2, alkanes, and alkenes. Passive trace gases have a chemical lifetime much greater than the transport time from the inflow measurement location near cloud base to the outflow measurement location near cloud top. Based on model simulations where trajectories are launched near cloud base, the transport time ranges from 10-60 minutes (Skamarock et al., 2000; Bela et al., 2018). It is preferable to use insoluble, passive trace gases that have a substantial difference in mixing ratio between the boundary layer and the free troposphere. Many previous studies have used CO as the insoluble, passive trace gas because it is a fast-response measurement (1 Hz) with small uncertainty (5%), has a low Henry's Law constant ($9.8x10^{-4}$ at 298 K), long chemical lifetime (typically > 1 month), and often higher mixing ratios in the boundary layer than the free troposphere. However, because of its long chemical lifetime, its free troposphere mixing ratios are not necessarily much smaller than its boundary layer mixing ratios. Thus, when possible, i-butane, n-butane, i-pentane, and n-pentane are used for this analysis. These alkanes meet the criteria for being insoluble with a chemical lifetime greater than 1-5 days. However, their collection time via the whole air sampler method ranges from 45 s to a few minutes with longer collection times at high altitude. The sampling of convective outflows during SEAC^{4}RS were less than a minute. Thus, CO and CO_2 are used to calculate the entrainment rate for the SEAC^{4}RS storms, except for the marine convection on 18 September 2013 where the entrainment rate is from a WRF calculation that simulated tracers at 1-km altitude layers (for more information see Cuchiara et al., 2023). Table S2 lists the trace gases used for the entrainment rate calculations. For most storm cases, the entrainment rate standard deviation is small compared to its average. More entrainment rate variation is seen for the 22 June 2012 and 18 September 2013 storms. Note that there is no systematic difference in entrainment rates when different trace gases are used (e.g., the entrainment rates using the alkanes as the passive, insoluble trace gas range from 4 to 15% km^{-1}, while the entrainment rates using CO and CO_2 range from 8 to 11% km^{-1}).

S2. Description of storm cases included in the analysis

18 May 2012 DC3 case

The 18 May 2012 case, sampled near Ogallala, Nebraska in the vicinity of a cold front, had a SWEAT Index of 283 categorizing it as a moderate, single cell storm. The storm was quite strong with respect to the 20 dBZ cloud top heights of 14 km MSL, reports of hail of one inch diameter (Herndon, 2012a), and periods of high lightning flash rates. The storm had relatively higher anthropogenic and agriculture signatures and lower biogenic signatures based on VOC measurements. The environment had a dry aerosol extinction of 31 Mm^{-1}, which is slightly higher than typical rural conditions (Barth et al., 2015). The BL *f(OA)* was 36%, underscoring the weaker influence of biogenic VOCs.

29 May 2012 DC3 case

The 29 May 2012 storm, sampled north of Oklahoma City, Oklahoma as a line of supercell storms, had a SWEAT Index of 422 producing large hail (up to 3 inch diameter) and a weak tornado. With its high convective available potential energy and 0-6 km wind shear, 20 dBZ cloud top heights exceeded 17 km MSL altitude. Vertical velocities exceeded 50 m s^{-1} (DiGangi et al., 2016). The central Oklahoma region has characteristics of both anthropogenic and biogenic VOCs with nearby oil and gas fields in central Oklahoma and north Texas, urban influences (Oklahoma City), and vegetation in eastern Oklahoma. The BL *f(OA)* was 53% and the dry aerosol extinction was 36 Mm^{-1}, slightly higher than typical rural conditions. This case is the same as that studied by Yang et al. (2015).

02 June 2012 DC3 case

On 2 June 2012, isolated convection was sampled between Greeley and Fort Morgan northeast of Denver, Colorado. The storm can be characterized as moderate convection (SWEAT Index of 256). While storm reports do not include observations of hail, there were reports of surface winds > 33 m s^{-1} (Herndon, 2012b). The 20 dBZ cloud top heights reached 15 km MSL. Like the 18 May 2012 case, the chemical environment showed signatures of anthropogenic influences from the Front Range of Colorado and smaller biogenic VOC mixing ratios. The dry aerosol extinction was low (12 Mm^{-1}) and the BL *f(OA)* was 58%.

06 June 2012 DC3 case

Convection on 6 June 2012 was associated with the "Denver cyclone," where low-level flow is southeasterly on the plains east of Denver and is northwesterly to the west of Denver, Colorado. The strong convection occurred just northeast of Denver and had a SWEAT Index of 296, 20 dBZ cloud top heights of 15 km MSL, and storm reports of one-inch diameter hail (Herndon, 2012b). Both the biogenic and anthropogenic VOC mixing ratios in the BL were low relative to other Colorado cases. The dry aerosol extinction was typical of rural background conditions (24 Mm^{-1}) and the BL *f(OA)* was 50%.

16 June 2012 DC3 case

Multicell convection occurred on 16 June 2012 in central Oklahoma. Its SWEAT Index of 360 categorized it as a severe storm. The 20 dBZ cloud top heights reached 15 km MSL. In contrast to the 29 May 2012 storm in Oklahoma,

both the anthropogenic and biogenic signatures of VOCs were low in the vicinity of this storm. The dry aerosol extinction was low (20 Mm^{-1}), typical of rural conditions. The BL *f(OA)* was 45%.

22 June 2012 DC3 case

The 22 June 2012 case had two severe convective storms occur along the Colorado-Nebraska border (at 41°N). The north storm was unique in that it ingested a wildfire smoke plume at 7 km MSL elevation, while the south storm did not ingest this smoke plume (Barth et al., 2015; Apel et al., 2015). The scavenging efficiency is estimated for only the south storm. The SWEAT Index for these storms was very high (442), cloud top heights reached 18 km MSL and there were reports of 1–2-inch hail for both storms (Herndon, 2012b). The smoke plume came from the High Park Fire west of Fort Collins, Colorado which had been burning for ~2 weeks. Biomass burning was occurring throughout the Rocky Mountain region resulting in its higher contribution to the atmospheric composition in the troposphere. The dry aerosol extinction was high (41 Mm^{-1}) for the region and BL *f(OA)* was 59%. Like other northeast Colorado storms, the biogenic VOCs were low relative to the anthropogenic VOCs (Barth et al., 2015).

02 September 2013 SEAC^{4}RS case

On 2 September 2013 a frontal system extending from north of the Great Lakes to southwest Texas was moving eastward across the US (Cuchiara et al., 2020). Associated with this front was the development of pre-frontal convection in Mississippi mostly of the form of airmass and multicell storms. The SWEAT Index calculated from the 1200 UTC Jackson, Mississippi NWS sounding was 214, while the SWEAT Index calculated from aircraft observations near the two storms was 225 for the airmass storm and 209 for the multicell storm (Table 1). In general, these storms were weaker than the storms sampled in Colorado and Oklahoma during DC3. The airmass and multicell storm cloud top heights were 8 km MSL and 13 km MSL, respectively, and the maximum radar reflectivity was lower in the airmass storm (45 dBZ) compared to the multicell storm (55 dBZ). The pre-frontal convection occurred mid-day (1800-1900 UTC; 1300-1400 LT) in a region rich in biogenic VOCs and low in anthropogenic VOCs (average BL mixing ratios were 1200 pptv isoprene and 39 pptv toluene). The dry aerosol extinction was high (47 Mm^{-1}) for the region with BL *f(OA)* of 54%.

18 September 2013 SEAC^{4}RS case

On 18 September 2013, the position of the "Bermuda High" pressure system over the mid-Atlantic coast and two low pressure systems over the Yucatan Peninsula and west coast of Mexico favored southeasterly flow from the Gulf of Mexico toward southern Texas giving moderate instability off the Texas coast and inland (Cuchiara et al., 2023). As a result, convection occurred over the Gulf of Mexico near Corpus Christi, Texas as well as to the south of San Antonio, Texas. The convection was sampled in the late morning to midday (16:00 – 19:00 UTC, 11:00 – 14:00 LT). To calculate the SWEAT Index, we used aircraft vertical profiles near the convection since the NWS Corpus Christi radiosonde occurred at least four hours before the convection was sampled. The SWEAT Index indicated weak to moderate convection for both the marine (SWEAT = 242) and land (SWEAT = 257) convection. The 20 dBZ cloud top heights for both marine and land convection reached 8 km MSL and the maximum radar reflectivities were 45-50 dBZ. Being in the same southeasterly flow, the chemical environment was clean for both marine and land convection. Average BL mixing ratios for isoprene and toluene were <60 pptv and the aerosol dry extinction was <12 Mm^{-1} over both the marine and land regions. This contrasts with the findings by Cuchiara et al. (2023) who reported differences

in cloud condensation nuclei (CCN) concentrations (282 cm^{-3} and 484 cm^{-3} in the marine and land convective inflow regions, respectively) and cloud characteristics of LWC, cloud base height, and updraft velocity. The BL *f(OA)* was 22% and 34% for the marine and land regions, respectively, which is smaller than the other cases analyzed in this study.

Supplementary Figures

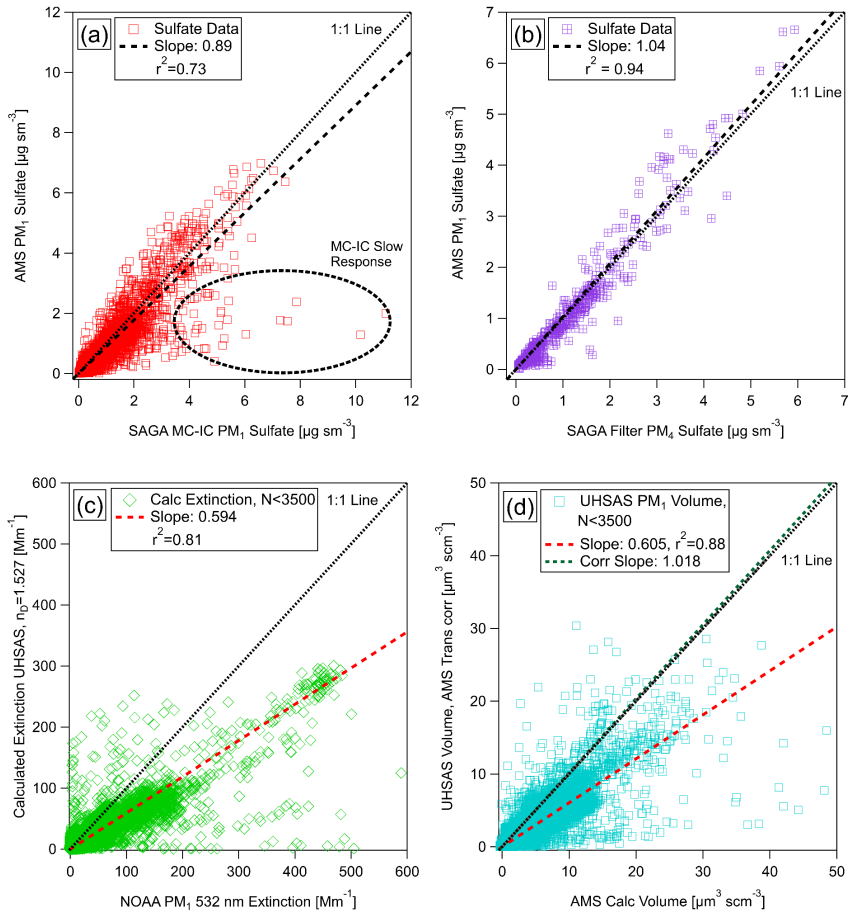

Figure S1: DC3 campaign-wide comparisons of selected aerosol chemical and physical properties as measured by a variety of in-situ sensors on the NASA DC-8. Data were averaged to the time scale of the slowest detector (SAGA Filter: 5-10 min; SAGA MC-IC: 75 s; UHSAS: 1 Hz; NOAA CRDS extinction: 1Hz) and points with less than 20% overlap have been discarded. Also not included are points where the CU aircraft AMS reported likely ice artifacts (see Section 2 in the main text). Panel (a) shows a comparison of aerosol sulfate reported by both the AMS and the SAGA mist-chamber ion chromatograph (MC-IC). The SAGA MC-IC instrument sometimes exhibits slow relaxation times when exiting plumes (Brock et al, 2019), which explains some of the scatter (circled area). Panel (b) shows the comparison of AMS sulfate and sulfate reported by the SAGA filter sampler, showing good agreement despite the very different time resolutions and duty cycles of both instruments. This also suggests that the overall contribution of organic sulfur to the AMS sulfate signal was small for the DC3 mission, although organosulfates were present (Liao et al., 2015). Panel (c) shows a comparison of calculated PM_1 aerosol extinction at 532 nm with the actual measurement by the NOAA CRDS instrument. The calculated aerosol extinction is based on the UHSAS size distribution, assuming no absorbing aerosol and an ambient refractive index close to the calibration aerosol (ammonium sulfate, nD=1.527) (Moore et al, 2021), consistent with findings from previous studies of the DC3 dataset (Aldhaif et al, 2018). UHSAS data were also filtered to exclude points where coincidence artifacts are likely (Kupc et al, 2018). While the correlation is quite robust (r^2=0.81) considering the assumptions, it has a consistent low bias. This bias is not present when using the AMS size distribution data (not shown). Panel (d) shows a comparison of calculated PM_1 chemical volume from the combined AMS and SP2 data with the physical volume data from the UHSAS, after applying a PM_1 transmission correction (see Guo et al, 2021 for details). The sub-100 nm SMPS volume is negligible (<1% on average) and is ignored because of the slow time resolution of that sensor (1 min). While the correlation is robust (r^2=0.88), there is again a low bias of almost the same magnitude as for the calculated extinction (also based on the UHSAS). If one assumes a systematic concentration bias in the reported UHSAS measurements of 40%, both the (independent) extinction and mass concentrations agree. We hence conclude that the AMS was consistent with the other in-situ optical and chemical sensors on the DC-8 and that there is no indication of major biases outside of the stated uncertainties.

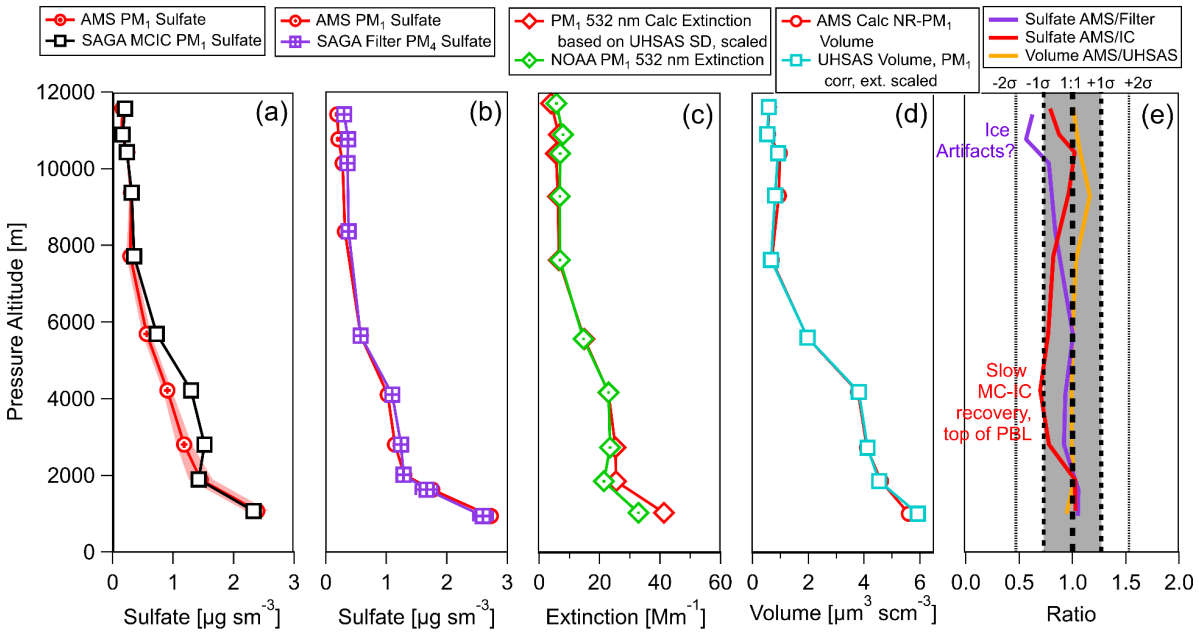

Figure S2: Campaign-wide altitude profiles of selected aerosol chemical and physical properties during the DC3 campaign as measured by a variety of in-situ sensors on the NASA DC-8. All profiles are based on the data shown in Fig. S1 (same averaging and filtering) and are reported as deciles for statistical consistency. They show (a) the comparison of the aerosol sulfate measurement from the AMS and SAGA filter measurements (b) same as (a) but using the sulfate from the SAGA MC-IC. (c) a comparison of the calculated and measured 532 nm extinction profiles (calculation details as in Fig S7), scaled assuming a 40% low bias in the UHSAS measurements, and (d) a comparison of AMS + BC calculated PM_1 volume with the physical volume reported by the (transmission corrected) UHSAS instrument, again corrected assuming a 40% low bias in the UHSAS measurements. Panel(e) summarizes the ratios of sulfate, extinction and volume for the different sensors. Also shown in (e) are the combined uncertainties of the AMS and each of the instruments being compared to as vertical lines (1:1 line, 1 sigma and 2 sigma uncertainty). Overall, within instrumental uncertainties there is no significant altitude bias in any of the reported data, and furthermore (except for the 40% low bias in the UHSAS measurements, independent of altitude) all aerosol sensors were generally consistent for the duration of the campaign. The two obvious deviations are 1) the low bias of AMS/MC-IC sulfate at 2-4 km altitude, which coincides with the top of the boundary layer and is due to the same slow recovery effect noted in Fig. S1, and 2) the low bias of AMS/Filter sulfate at 12 km altitude. While there were often dust layers at 6-8 km (per HSRL measurements) they are unlikely to explain this difference at 10-12 km altitude. Given the consistency for the other sensor comparisons, this could be due to inlet/ice impaction artifacts (Murphy et al., 2004). It should be noted that all sensors except volume and extinction used dedicated inlets and hence are likely to be affected differently by such artifacts.

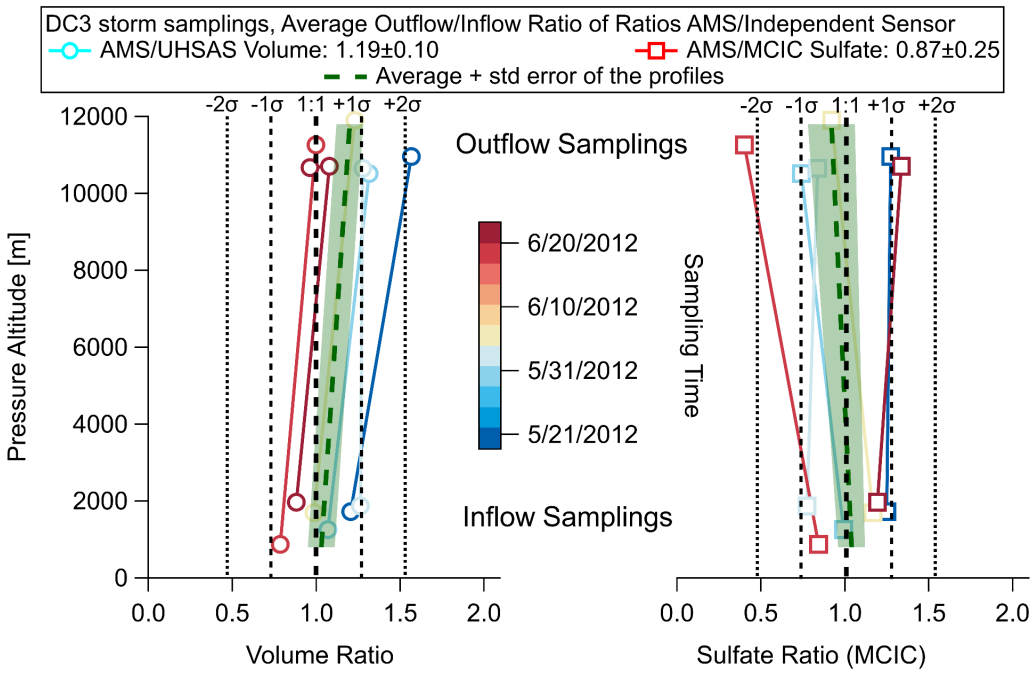

Figure S3: Calculated ratios of volume and sulfate from the UHSAS and MC-IC sensors in the inflow and outflow regions analyzed in this work for the DC3 mission (the SEAC[4]RS cases are too short to be included here), compared (as in Fig. S2) to the reported combined uncertainties of the CU aircraft AMS and the sensor being compared to (1:1 line, 1 sigma and 2 sigma uncertainty). No extinction measurements were reported in the outflow of these storms and hence are not included here. Likewise, the overlap of the outflow periods with the filter measurements was generally low (<25%) and is not included here. The consistency of the outflow measurements is lower than the overall consistency of the high-altitude measurements shown in Fig. S2 and may be affected by the different responses of each sensor to ice artifacts. Importantly, none of the storms have a clear discernible bias across all sensors. This is also the case if one takes the average of the dataset, as illustrated by the average of the outflow to inflow ratios (green line/shaded green area). The average bias for the two sensors shown is of opposite sign and overall, including their statistical error, still well within combined instrument uncertainties. Hence, these uncertainties very likely represent well the uncertainties in scavenging efficiencies presented in this work.

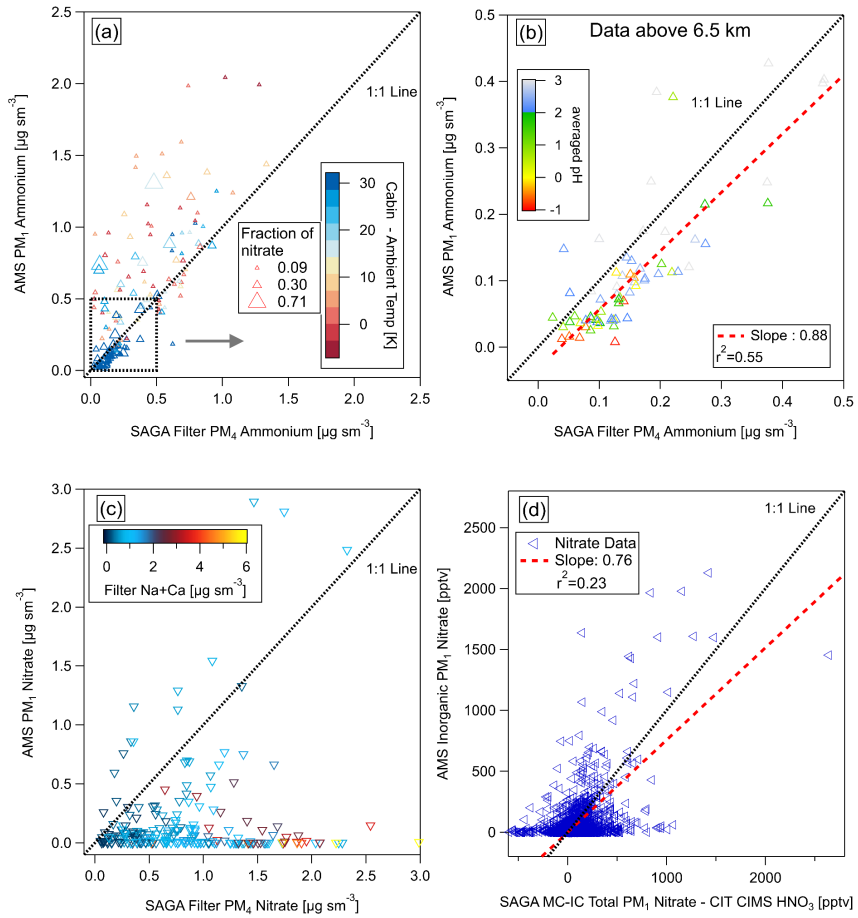

Figure S4: Comparisons of other CU aircraft AMS data products with co-located chemical aerosol measurements where comparisons are generally less robust and meaningful than sulfate for different reasons. Panels (a) and (b) both show the correlation of PM_1 ammonium with PM_4 sulfate from the SAGA filter measurements. Panel (a) suggests significant evaporation of ammonium from the filter substrate anytime the aircraft cabin temperature was higher than ambient and/or the ammonium nitrate fraction in the aerosol was high. This is consistent with previous observations reported in Heim et al (2020). Panel (b), a subset of panel (a) as shown by the dashed square, on the other hand shows the filter sampler reporting higher ammonium in the upper troposphere, particularly when aerosol pH is low. This is consistent with previous findings reported in Nault et al (2020) for the ATom, DC3, and SEAC^{4}RS campaigns. Panel (c) shows a comparison of AMS and filter nitrate, the latter is consistently higher in most plumes and is typically associated with enhanced sodium and calcium concentrations, suggesting that this is mostly coarse nitrate, likely from dust which is outside the size range of the AMS. Panel (d) shows a comparison of AMS apportioned inorganic nitrate with the difference between the SAGA MC-IC total nitrate measurement (aerosol inorganic nitrate + nitric acid) and the nitric acid measurement from the CIT-CIMS. This comparison is affected by the delayed response of the SAGA MC-IC sensor when exiting plumes and the different sampling times (1Hz with blanks for the CIT-CIMS versus 75 s for the MC-IC sensor), which likely explain the scatter around the AMS zero. Overall, there is reasonable consistency between the three sensors.

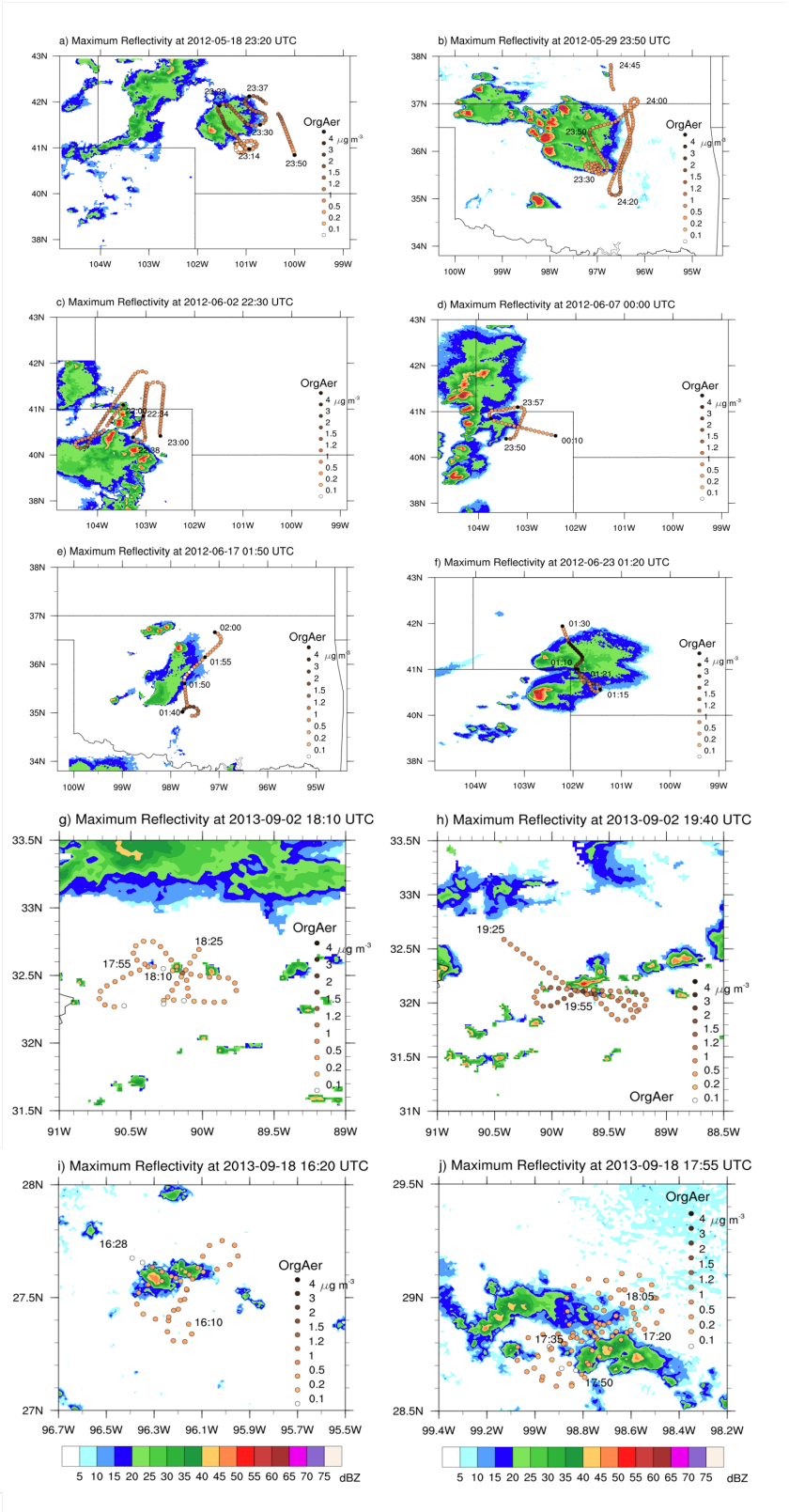

Figure S5. Maximum radar reflectivity in each vertical column for the ten cases analyzed, a) 18 May 2012, b) 29 May 2012, c), 2 June 2012, d) 6 June 2012, e) 16 June 2012, f) 22 June 2012, g) 2 September 2013 air mass storm, h) 2 September 2013 multicell storm, i) 18 September 2013 Gulf of Mexico storm, and j) 18 September 2013 South Texas storm. Overlaid is the DC-8 flight track in the storm outflow colored by the organic aerosol mass concentration (μg std m^{-3}).

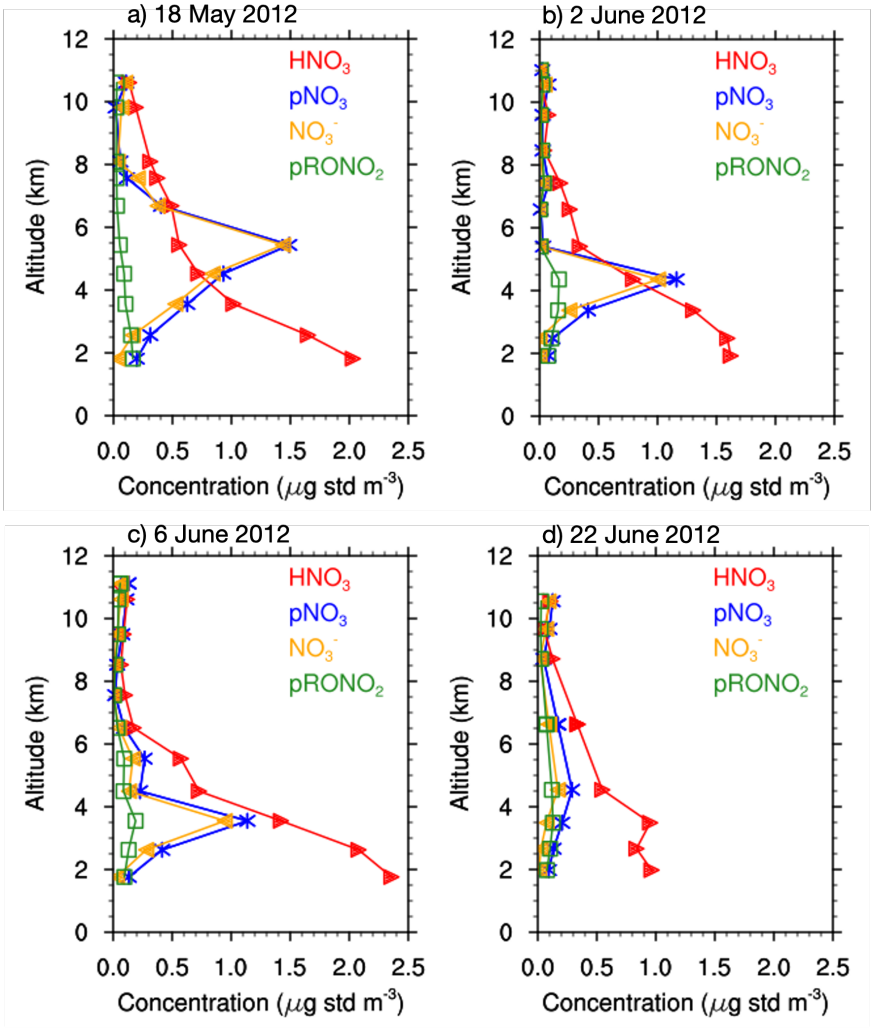

Figure S6. Clear air vertical profiles of HNO_3 (red), particulate nitrate (blue), inorganic particulate nitrate (gold), and organic particulate nitrate (green) for a) 18 May 2012, b) 2 June 2012, c) 6 June 2012, and d) 22 June 2012 DC3 storms.

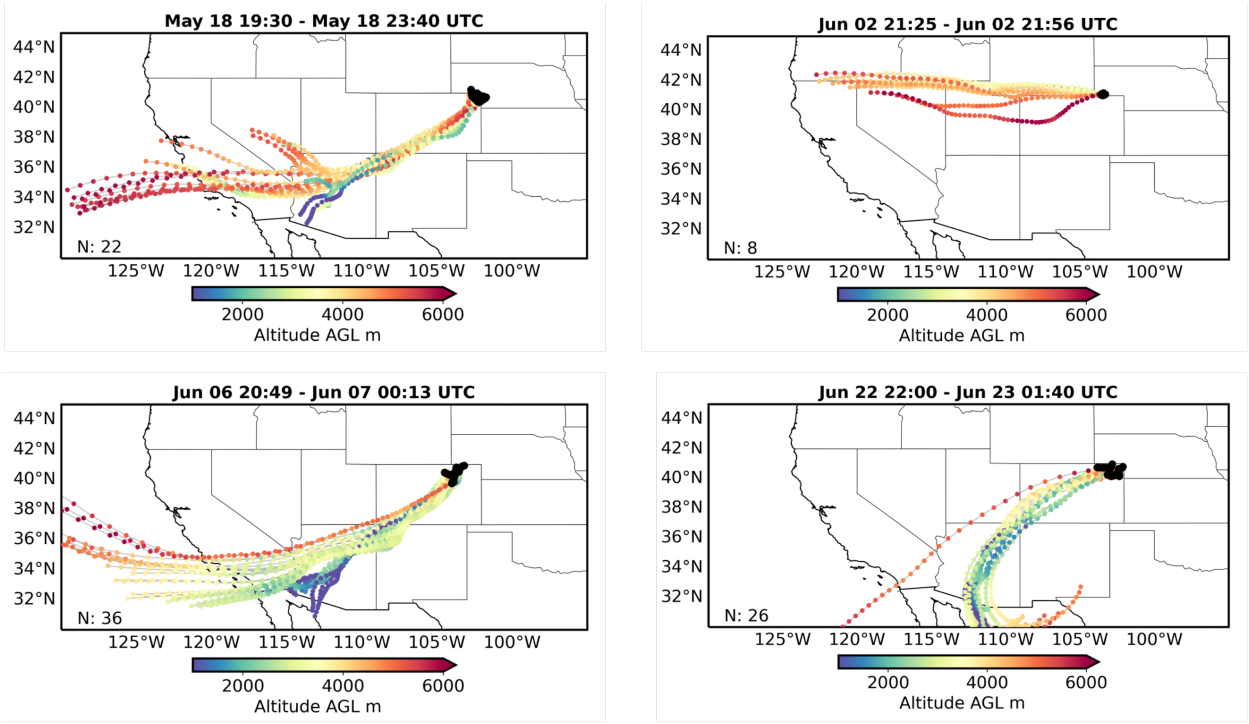

Figure S7. HYSPLIT 48-hour back trajectories calculated for four DC3 storms.

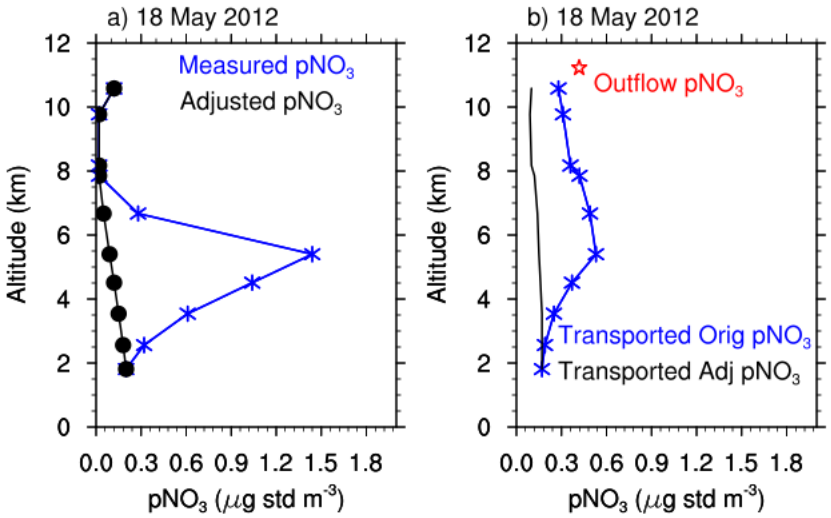

Figure S8. Vertical profiles of particulate nitrate (left) that were measured (blue) and adjusted to remove the mid-troposphere layer (black) and of transported particulate nitrate calculated by the entrainment model (right) with calculated values using the measured clear sky vertical profile (blue) and those using the adjusted clear sky vertical profile (black) for the 18 May 2012 case. The red circle marks the measured concentration of the outflow particulate nitrate concentration.

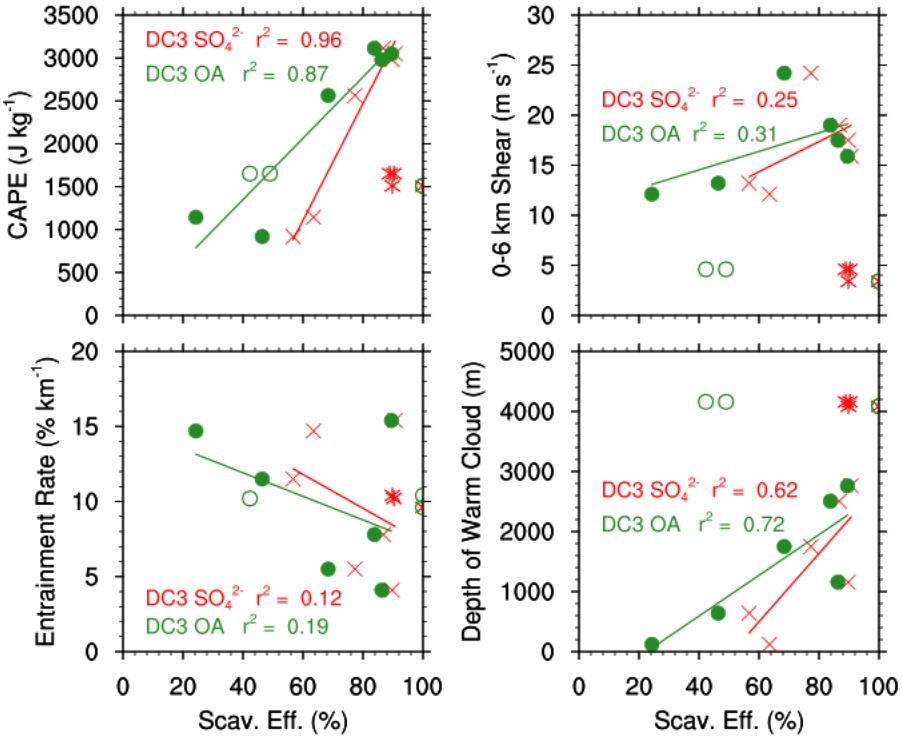

Figure S9. Scatter plots of SO_4^{2-} (red) and OA (green) scavenging efficiencies with various storm parameters (upper left: CAPE; upper right: 0-6 km wind shear; lower left: entrainment rate; lower right: depth from cloud base to 0°C). The DC3 storms are red x markers and solid green circles for SO_4^{2-} and OA, respectively, and the SEAC^{4}RS storms are red asterisks and open green circles for SO_4^{2-} and OA, respectively. The CAPE, wind shear, and warm cloud depth are from DC3 radiosondes or NWS radiosondes. The correlation coefficients are based on only the DC3 storms.

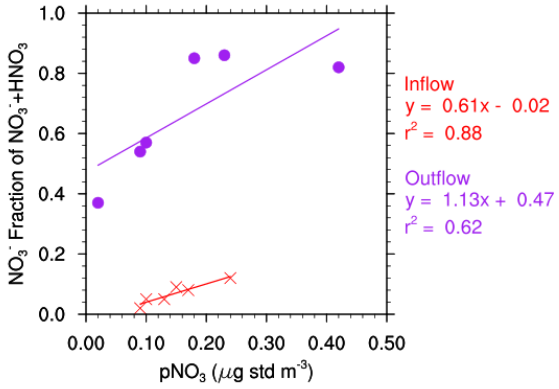

Figure S10. Scatter plot of pNO3 and the NO_3^- fraction of NO_3^- + HNO_3 for the six DC3 cases. Purple solid circles are for the convective outflow regions and red crosses are for the inflow regions.

Supplementary Tables

Table S1. List of data and instruments used in the analysis.

Species/Parameter	Instrument[a]	Uncertainty	Reference
SO_4^{2-}, NH_4^+, NO_3^-, OA, *m*/z 44 for submicron aerosol mass	CU aircraft AMS	Inorganics 34%, Organics 38% (2 sigma)	DeCarlo et al. (2006), Guo et al. (2021)
CO	DACOM	5% or 1 ppmv	Sachse et al. (1987)
CO_2	AVOCET	0.25 ppmv	Vay et al. (2011)
n-butane, i-butane, n-pentane, i-pentane, isoprene, toluene	WAS	5% or 3 pptv	Simpson et al. (2011)
isoprene, toluene	PTR-MS	5%	de Gouw and Warneke (2007)
Aerosol dry extinction at 532 nm	NASA/LaRC optical aerosol measurements	5%	Wagner et al. (2015)
BC	HD-SP2	30%	Schwarz et al. (2013)
HCN	CIT-CIMS	50% + 50 pptv	Crounse et al. (2006)
CH_3CN	PTR-MS	25 pptv	de Gouw and Warneke (2007)
MPN, ANs, PNs	TD-LIF	MPN, ANs: 15% PNs: 10%	Nault et al. (2015)
HNO_3	CIT-CIMS	30% + 50 pptv	Crounse et al. (2006)
O_3	CSD CL	0.040 ppbv + 3%	Ryerson et al. (2000); Pollack et al. (2011)
OH	ATHOS	32%	Faloona et al. (2004)
Aerosol number	SMPS	10%	Wang and Flagan (1990)
SO_4^{2-}, NH_4^+, NO_3^-, Ca^{2+}, Na^+ (PM_4)	SAGA Filter Sampler	20%	Dibb et al. (1999), McNaughton et al. (2007)
SO_4^{2-}, total nitrate (PM_1)	SAGA MC-IC	20%	Scheuer et al. (2003)
Aerosol Volume	NASA/LaRC UHSAS Spectrometer	20%	Cai et al. (2008), Kupc et al. (2018)
Aerosol extinction	CRDS	3%	Langridge et al. (2011)
Pressure, Temperature, 3D Winds	MMS	Pressure: 0.5% Temperature: 0.2% Winds: 3%	Chan et al. (1998)
Ice water content	2D-S	Not available	Lawson (2011)

[a]CU-HR-TOF-AMS is the University of Colorado High Resolution, Time of Flight, Aerosol Mass Spectrometer; DACOM is the Differential Absorption CO Measurement; AVOCET is the Atmospheric Vertical Observation of CO2 in the Earth's Troposphere; WAS is the Whole Air Sampler that uses gas chromatography; PTR-MS is the Institut fuer Ionenphysik und Angewandte Physik Proton Transfer Mass Spectrometer; HD-SP2 is the Humidified Dual Single Particle Soot Photometer; CIT-CIMS is California Institute of Technology chemical ionization mass spectrometry; TD-LIF is thermal dissociation – laser induced fluorescence; CSD CL is NOAA Chemical Science Division chemiluminescence; ATHOS is the Airborne Tropospheric Hydrogen Oxides Sensor; SMPS is the Scanning

Mobility Particle Sizer; SAGA is Soluble Acidic Gases and Aerosols; SAGA MC-IC is SAGA mist chamber – ion
255 chromatography; UHSAS is Ultra-High Sensitivity Aerosol size Spectrometer; CRDS is Cavity Ringdown extinction Spectrometer; MMS is Meteorological Measurement System; 2D-S is two-dimensional stereo probe.

Table S2. NASA DC-8 aircraft inflow and outflow times, and their associated altitudes for each storm analyzed.

Campaign and Date (mm/dd/yy)	Inflow Altitude (km)	Inflow Time (UTC)	Outflow Altitude (km)	Outflow Time (UTC)
DC3 05/18/12	1.7	22:48:29-22:51:10	11.3	23:17:50-23:22:00
DC3 05/29/12	1.3	23:10:21-23:15:53	11.0	23:48:30-23:58:13
DC3 06/02/12	1.9	21:16:18-21:27:38	11.1	22:34:14-22:46:10
DC3 06/06/12	1.7	22:13:40-22:25:12	12.4	23:56:00-24:10:00 [a]
DC3 06/16/12	0.95	24:15:00-24:20:00 [a]	11.9	25:50:00-25:55:00[a]
DC3 06/22/12	2.0	22:31:27-22:45:54	11.2	25:13:52-25:14:38 [a] 25:16:51-25:19:24 [a]
SEAC^{4}RS 09/02/13 Airmass	0.8	16:53:11-16:53:551	8.0 8.0 8.0	18:09:45-18:10:15 18:16:03-18:16:32 18:23:16-18:23:33
SEAC^{4}RS 09/02/13 Multicell	0.4	22:12:01-22:18:14	12.0 12.0	19:31:10-19:31:55 19:53:34-19:54:11
SEAC^{4}RS 09/18/13 Marine	0.6	15:38:35-15:39:18	8.1 8.1 8.1	16:15:13-16:15:16 16:20:34-16:20:36 16:21:01-16:21:10
SEAC^{4}RS 09/18/13 Land Core 2	0.9	18:30:58-18:35:38	10.1 10.2 10.7 11.3 12.0	17:16:40-17:16:47 17:17:01-17:17:19 17:22:23-17:22:30 17:27:48-17:27:58 17:35:31-17:35:40
SEAC^{4}RS 09/18/13 Land Core 3	0.9	18:30:58-18:35:38	12.0 11.1	17:40:28-17:40:41 17:46:39-17:46:48 17:59:00-17:59:10

[a]The nomenclature for the hour of 24 and 25 refers to hour 00 and 01 on the next day.

Table S3. Trace gases used for the entrainment rate calculation for each storm and the entrainment rate average ± standard deviation among the 2-4 trace gases used for its calculation.

Date	Insoluble, Passive Trace Gases	Entrainment Rate (% km^{-1})
	DC3	
18 May 2012	i-,n-butane, i-,n-pentane	14.7 ± 0.2
29 May 2012	i-,n-butane, i-,n-pentane	7.8 ± 0.9
02 June 2012	CO	11.5
06 June 2012	i-,n-butane, i-,n-pentane	4.1± 0.7
16 June 2012	i-,n-butane, i-,n-pentane	15.4 ± 1.2
22 June 2012	i-,n-butane, n-pentane	5.5 ± 2.0
	SEAC^{4}RS	
02 Sept 2013	CO, CO_2	11.4 ± 1.6
02 Sept 2013	CO, CO_2	8.3 ± 1.6
18 Sept 2013 Marine	WRF tracer calculation	9.6 ± 3.2
18 Sept 2013 Land, core 2	CO, CO_2	7.8 ± 5.2
18 Sept 2013 Land, core 3	CO, CO_2	10.4 ± 5.4

Table S4. Inflow, outflow, and calculated aerosol concentrations (μg std m^{-3}) for each case and the estimated scavenging efficiency (%) given as averages ± standard deviation.

Date	Measured Inflow Concentration[a]	Measured Outflow Concentration[a]	Calculated Cloud Top Concentration[b]	Scavenging Efficiency[b,c,d]
		Sulfate		
18 May 2012	2.93 ± 0.50	0.44 ± 0.14	1.18	62.9 ± 7.4
29 May 2012	2.11 ± 0.36	0.16 ± 0.08	1.08	86.8 ± 3.2
02 June 2012	0.80 ± 0.14	0.18 ± 0.08	0.42	56.5 ± 8.4
06 June 2012	2.00 ± 0.34	0.16 ± 0.07	1.32	89.6 ± 2.5
16 June 2012	1.58 ± 0.27	0.06 ± 0.05	0.67	90.7 ± 1.9
22 June 2012	1.33 ± 0.23	0.26 ± 0.06	1.04	75.2 ± 7.9
02 Sept 2013[e]	3.45 ± 0.59	0.10 ± 0.03	1.61	95.0 ± 1.2
02 Sept 2013	3.22 ± 0.55	0.12 ± 0.04	1.57	92.7 ± 1.9
18 Sept 2013[e]	1.71 ± 0.37	*0.11 ± 0.06*	0.89	100
18 Sept 2013[e]	1.48 ± 0.45	0.07 ± 0.04	0.77	90.7 ± 4.9
18 Sept 2013[e]	1.48 ± 0.45	0.07 ± 0.02	0.57	87.9 ± 7.0
		Ammonium		
18 May 2012	1.15 ± 0.20	0.31 ± 0.09	0.51	39.2 ± 12.0
29 May 2012	0.87 ± 0.15	0.09 ± 0.03	0.43	81.3 ± 4.6
02 June 2012	0.33 ± 0.06	0.12 ± 0.05	0.18	37.0 ± 12.3
06 June 2012	0.72 ± 0.12	0.08 ± 0.02	0.49	86.0 ± 3.4
16 June 2012	0.58 ± 0.10	0.03 ± 0.02	0.24	87.6 ± 2.5
22 June 2012	0.50 ± 0.08	0.15 ± 0.04	0.44	65.3 ± 9.7
02 Sept 2013[e]	0.95 ± 0.16	*0.02 ± 0.01*	0.41	100
02 Sept 2013	0.83 ± 0.14	0.08 ± 0.06	0.40	80.9 ± 4.9
18 Sept 2013[e]	0.10 ± 0.03	*0.001 ± 0.001*	0.05	100
18 Sept 2013	0.40 ± 0.10	*0.001 ± 0.004*	0.19	100
18 Sept 2013	0.40 ± 0.10	*0.001 ± 0.006*	0.13	100
		Nitrate		
18 May 2012	0.17 ± 0.05	0.42 ± 0.10	0.28	–
29 May 2012	0.24 ± 0.04	0.09 ± 0.05	0.13	40.5 ± 13.7
02 June 2012	0.10 ± 0.02	0.18 ± 0.08	0.13	–
06 June 2012	0.13 ± 0.03	0.10 ± 0.05	0.17	41.9 ± 10.6
16 June 2012	0.15 ± 0.03	*0.02 ± 0.04*	0.13	82.8 ± 3.1
22 June 2012	0.09 ± 0.03	0.23 ± 0.06	0.21	–
02 Sept 2013[e]	0.18 ± 0.04	0.06 ± 0.05	0.08	42.9 ± 13.5
02 Sept 2013	0.07 ± 0.03	0.31 ± 0.20	0.08	–
18 Sept 2013[e]	*0.03 ± 0.01*	*0.01 ± 0.01*	0.02	NaN
18 Sept 2013	0.08 ± 0.07	*0.03 ± 0.03*	0.04	100
18 Sept 2013	0.08 ± 0.07	*0.03 ± 0.01*	0.03	100
		Organic Aerosol		
18 May 2012	6.05 ± 1.15	1.80 ± 0.83	2.51	28.9 ± 15.8
29 May 2012	8.76 ± 1.66	0.71 ± 0.50	4.05	84.5 ± 4.4
02 June 2012	3.48 ± 0.66	0.88 ± 0.46	1.68	48.0 ± 11.7
06 June 2012	4.89 ± 0.93	0.49 ± 0.29	3.28	86.7 ± 3.6
16 June 2012	4.12 ± 0.78	0.19 ± 0.39	1.80	89.5 ± 2.3
22 June 2012	5.80 ± 1.10	1.64 ± 0.75	4.88	66.2 ± 11.1
02 Sept 2013[e]	5.92 ± 1.13	0.54 ± 0.58	2.82	84.4 ± 4.0
02 Sept 2013	6.46 ± 1.51	1.36 ± 0.74	3.20	57.6 ± 11.7
18 Sept 2013[e]	0.66 ± 0.18	*0.31 ± 0.16*	0.42	100
18 Sept 2013	1.05 ± 0.33	*0.31± 0.21*	0.55	100
18 Sept 2013	1.05 ± 0.33	*0.31 ± 0.32*	0.43	100

[a]Average concentrations below the detection limit are shown in italics. Variability is the maximum of the standard deviation or the uncertainty of the AMS measurement.

[b]For cases where the outflow leg is below the detection limit, the scavenging efficiency is shown as 100% and an uncertainty is not assigned since the measured outflow concentration is not statistically different from zero.

[c]Variability is the maximum of the standard deviation caused by the entrainment rate variability (Table S2) or the propagation of the uncertainty of the AMS measurement.
[d]For cases marked with a dash, the scavenging efficiency is not given because the outflow concentration is greater than the inflow concentration. The case marked NaN is not a number because both the inflow and outflow measured concentrations are below the detection limit.
[e]Measurements from the outflow intercepts were combined to have a larger sample size for the scavenging efficiency calculation.

Table S5. Inorganic nitrate partitioning ratios: $NO_3^-/(NO_3^-+HNO_3)$.

Date	Inflow	Outflow
18 May 2012	0.08	0.82
29 May 2012	0.12	0.54
02 June 2012	0.05	0.85
06 June 2012	0.05	0.57
16 June 2012	0.09	0.37
22 June 2012	0.02	0.86

Table S6. Inflow and outflow particulate inorganic nitrate (NO_3^-), and particulate organic nitrate ($pRONO_2$) average ± standard deviation concentrations (μg std m^{-3}) and their estimated scavenging efficiency (%) for the DC3 cases.

Date	Measured Inflow Concentration[a]	Measured Outflow Concentration[a]	Scavenging Efficiency[b]
	NO_3^-		
18 May 2012	0.02 ± 0.02	0.31 ± 0.14	–
29 May 2012	0.07 ± 0.01	0.03 ± 0.01	42.6
02 June 2012	*0.00 ± 0.00*	0.11 ± 0.01	–
06 June 2012	0.03 ± 0.01	0.04 ± 0.02	39.8
16 June 2012	*0.00 ± 0.00*	–	–
22 June 2012	0.01 ± 0.01	0.15 ± 0.01	–
	$pRONO_2$		
18 May 2012	0.16 ± 0.02	0.13 ± 0.08	–
29 May 2012	0.16 ± 0.03	0.05 ± 0.03	56.9
02 June 2012	0.09 ± 0.01	0.07 ± 0.03	10.5
06 June 2012	0.09 ± 0.01	0.05 ± 0.02	35.7
16 June 2012	0.15 ± 0.02	–	–
22 June 2012	0.08 ± 0.01	0.06 ± 0.01	17.2[c]

[a]Concentrations where total particulate nitrate (pNO_3) was greater than the detection limit but apportioned NO_3^- or $pRONO_2$ was below the detection limit are shown in italics. An apportionment is not possible when pNO_3 is below the detection limit (Day et al., 2022); these cases are marked as missing values.
[b]Unreported scavenging efficiencies are due to outflow concentrations being greater than inflow concentrations or the calculated cloud top concentration is less than the outflow concentration (18 May 2012 case for $pRONO_2$).
[c]Uncertain result as the clear-sky concentrations contained missing data in the mid-troposphere that was filled with the average clear sky concentration between two altitudes.

References

Aldhaif, A. M., Stahl, C., Braun, R. A., Moghaddam, M. A., Shingler, T., Crosbie, E., Sawamura, P., Dadashazar, H., Ziemba, L., Jimenez, J. L., Campuzano-Jost, P., and Sorooshian, A.: Characterization of the real part of dry aerosol refractive index over North America from the surface to 12 km, J. Geophys. Res. D: Atmos., 123, 8283–8300, doi:10.1029/2018JD028504, 2018.

Apel, E. C., Hornbrook, R. S., Hills, A. J., Blake, N. J., Barth, M. C., Weinheimer, A., Cantrell, C., Rutledge, S. A., Basarab, B., Crawford, J., Diskin, D., Homeyer, C. R., Campos, T., Flocke, F., Fried, A., Blake, D. R., Brune, W., Pollack, I., Peischl, J., Ryerson, T., Wennberg, P. O., Crounse, J. D., Wisthaler, A., Mikoviny, T., Huey, G., Heikes, B., O'Sullivan D., and Riemer, D. D.: Upper tropospheric ozone production from lightning NOx-impacted convection: Smoke ingestion case study from the DC3 campaign, J. Geophys. Res., 120, 2505– 2523, doi:10.1002/2014JD022121, 2015.

Barth, M. C., Cantrell, C. A., Brune, W. H., Rutledge, S. A., Crawford, J. H., Huntrieser, H., Carey, L. D., MacGorman, D., Weisman, M., Pickering, K. E., Bruning, E., Anderson, B., Apel, E., Biggerstaff, M., Campos, T., Campuzano-Jost, P., Cohen, R., Crounse, J., Day, D. A., Diskin, G., Flocke, F., Fried, A., Garland, C., Heikes, B., Honomichl, S., Hornbrook, R., Huey, L. G., Jimenez, J., Lang, T., Lichtenstern, M., Mikoviny, T., Nault, B., O'Sullivan, D., Pan, L., Peischl, J., Pollack, I., Richter, D., Riemer, D., Ryerson, T., Schlager, H., St. Clair, J., Walega, J., Weibring, P., Weinheimer, A., Wennberg, P., Wisthaler, A., Wooldridge, P., and Ziegler, C.: The Deep Convective Clouds and Chemistry (DC3) field campaign, Bull. Amer. Meteor. Soc., 96, 1281–1309, doi:10.1175/BAMS-D-13-00290.1, 2015.

Barth, M. C., Bela, M. M., Fried, A., Wennberg, P., Crounse, J., St. Clair, J., Blake, N., Blake, D. R., Homeyer, C. R., Brune, W. H., Zhang, L., Mao, J., Ren, X., Ryerson, T., Pollack, I. B., Peischl, J., Cohen, R. C., Nault, B. A., Huey, L. G., Liu, X., and Cantrell, C. A.: Convective transport and scavenging of peroxides by thunderstorms observed over the Central U.S. during DC3, J. Geophys. Res., 121, 4272– 4295, doi:10.1002/2015JD024570, 2016.

Bela, M. M., Barth, M. C., Toon, O. B., Fried, A., Ziegler, C., Cummings, K. A., Li, Y., Pickering, K. E., Homeyer, C. R., Morrison, H., Yang, Q., Mecikalski, R. M., Carey, L., Biggerstaff, M. I., Betten, D. P., and Alford, A. A.: Effects of scavenging, entrainment, and aqueous chemistry on peroxides and formaldehyde in deep convective outflow over the central and Southeast U.S., J. Geophys. Res., 123, 7594– 7614, doi:10.1029/2018JD028271, 2018.

Brock, C. A., Williamson, C., Kupc, A., Froyd, K. D., Erdesz, F., Wagner, N., Richardson, M., Schwarz, J. P., Gao, R.-S., Katich, J. M., Campuzano-Jost, P., Nault, B. A., Schroder, J. C., Jimenez, J. L., Weinzierl, B., Dollner, M., Bui, T., and Murphy, D. M.: Aerosol size distributions during the Atmospheric Tomography Mission (ATom): Methods, uncertainties, and data products, Atmos. Meas. Tech., 12, 3081–3099, doi:10.5194/amt-12-3081-2019, 2019.

Cai, Y., Montague, D. C., Mooiweer-Bryan, W., Deshler, T., Mooiweerbryan, W., and Deshler, T.: Performance characteristics of the ultra high sensitivity aerosol spectrometer for particles between 55 and 800nm: Laboratory and field studies, J. Aerosol Sci., 39, 759–769, doi:10.1016/j.jaerosci.2008.04.007, 2008.

Chan, K. R., Dean-Day, J., Bowen, S. W., and Bui, T. P.: Turbulence measurements by the DC-8 meteorological measurement system. Geophys.Res. Lett., 25(9), 1355–1358. doi:10.1029/97GL03590, 1998.

Crounse, J. D., McKinney, K. A., Kwan, A. J., and Wennberg, P. O.: Measurement of gas-phase hydroperoxides by chemical ionization mass spectrometry. Analytical Chemistry, 78(19), 6726–6732. doi:10.1021/ac0604235, 2006.

Cuchiara, G. C., Fried, A., Barth, M. C., Bela, M., Homeyer, C. R., Gaubert, B., Walega, J., Weibring, P., Richter, D., Wennberg, P., Crounse, J., Kim, M., Diskin, G., Hanisco, T. M., Wolfe, G. M., Beyersdorf, A., Peischl, J., Pollack, I. B., St. Clair, J. M., Woods, S., Tanelli, S., Bui, T. P., Dean-Day, J., Huey, G. L., and Heath, N.: Vertical transport, entrainment, and scavenging processes affecting trace gases in a modeled and observed SEAC^{4}RS case study. J. Geophys. Res., 125, e2019JD031957, doi.org/10.1029/2019JD031957, 2020.

Cuchiara, G. C., Fried, A., Barth, M. C., Bela, M., Homeyer, C. R., Walega, J., Weibring, P., Richter, D., Woods, S., Beyersdorf, A., Bui, T. P., Dean-Day, J.: Effect of marine and land convection on wet scavenging of ozone

precursors observed during a SEAC[4]RS case study, J. Geophys. Res., 28, e2022JD037107, doi:10.1029/2022JD037107, 2023.

Day, D. A., Campuzano-Jost, P., Nault, B. A., Palm, B. B., Hu, W., Guo, H., Wooldridge, P. J., Cohen, R. C., Docherty, K. S., Huffman, J. A., de Sá, S. S., Martin, S. T., and Jimenez, J. L.: A systematic re-evaluation of methods for quantification of bulk particle-phase organic nitrates using real-time aerosol mass spectrometry, Atmos. Meas. Tech., 15, 459–483, doi:10.5194/amt-15-459-2022, 2022.

DeCarlo, P., Kimmel, J., Trimborn, A., Northway, M., Jayne, J., Aiken, A., Gonin, M., Fuhrer, K., Horvath, T., Docherty, K., Worsnop, D., and Jimenez, J.: Field-deployable, high-resolution, time-of-flight aerosol mass spectrometer, Anal. Chem., 78, 8281–8289, doi:10.1021/ac061249n, 2006.

de Gouw, J. and Warneke, C:, Measurements of volatile organic compounds in the Earth's atmosphere using proton-transfer-reaction mass spectrometry, Mass Spectrom. Rev., 26, 223–257, doi:10.1002/mas.20119, 2007.

Dibb, J. E., Talbot, R. W., Scheuer, E. M., Blake, D. R., Blake, N. J., Gregory, G. L., Sachse, G. W., and Thornton, D. C.: Aerosol chemical composition and distribution during the Pacific Exploratory Mission (PEM) Tropics, J. Geophys. Res.,, 104, 5785–5800, doi:10.1029/1998JD100001, 1999.

DiGangi, E. A., MacGorman, D. R., Ziegler, C. L., Betten, D., Biggerstaff, M., Bowlan, M., and Potvin, C. K.: An overview of the 29 May 2012 Kingfisher supercell during DC3, J. Geophys. Res. Atmos., 121, 14,316–14,343, doi:10.1002/2016JD025690, 2016.

Faloona, I. C., Tan, D., Lesher, R. L., Hazen, N. L., Frame, C. L., Simpas, J. B., Harder, H., Martinez, M., Di Carlo, P., Ren, X. R., and Brune, W. H.: A laser-induced fluorescence instrument for detecting tropospheric OH and HO_2: Characteristics and calibration, J. Atmos. Chem., 47, 139–167, doi:10.1023/B:JOCH.0000021036.53185.0e, 2004.

Fried, A., Barth, M. C., Bela, M., Weibring, P., Richter, D., Walega, J., Li, Y., Pickering, K. E., Apel, E., Hornbrock, R. S., Hills, A., Riemer, D. D., Blake, N., Blake, D., Schroeder, J. R., Luo, Z. J., Crawford, J. H., Olson, J., Rutledge, S., Betten, D., Biggerstaff, M. I., Diskin, G., Sachse, G., Campos, T., Flocke, F., Weinheimer, A., Cantrell, C., Pollack, I., Peischl, J., Froyd, K., Wisthaler, A., Mikoviny, T. and Woods, S.: Convective Transport of formaldehyde to the upper troposphere and lower stratosphere and associated scavenging in thunderstorms over the Central United States during the 2012 DC3 study, J. Geophys. Res., 120, 7430– 7460, doi:10.1002/2015JD024477, 2016.

Guo, H., Campuzano-Jost, P., Nault, B. A., Day, D. A., Schroder, J. C., Kim, D., Dibb, J. E., Dollner, M., Weinzierl, B., Jimenez, J. L.: The importance of size ranges in aerosol instrument intercomparisons: a case study for the Atmospheric Tomography Mission, Atmos. Meas. Tech., 14, 3631–3655, doi:10.5194/amt-14-3631-2021, 2021.

Heim, E. W., Dibb, J., Scheuer, E., Jost, P. C., Nault, B. A., Jimenez, J. L., Peterson, D., Knote, C., Fenn, M., Hair, J., Beyersdorf, A. J., Corr, C., and Anderson, B. E.: Asian dust observed during KORUS-AQ facilitates the uptake and incorporation of soluble pollutants during transport to South Korea, Atmos. Environ., 224, 117305, doi:10.1016/j.atmosenv.2020.117305, 2020.

Herndon, R.: "Storm Data and Unusual Weather Phenomena", National Climatic Data Center, 54, (5), 2012a.

Herndon, R.: "Storm Data and Unusual Weather Phenomena", National Climatic Data Center, 54, (6), 2012b.

Kupc, A., Williamson, C., Wagner, N. L., Richardson, M., and Brock, C. A.: Modification, calibration, and performance of the ultra-high sensitivity aerosol spectrometer for particle size distribution and volatility measurements during the Atmospheric Tomography Mission (ATom) airborne campaign, Atmos. Meas. Tech., 11, 369–383, doi:10.5194/amt-11-369-2018, 2018.

Langridge, J. M., Richardson, M. S., Lack, D., Law, D., & Murphy, D. M.: Aircraft instrument for comprehensive characterization of aerosol optical properties, Part I: Wavelength-dependent optical extinction and its relative humidity dependence measured using cavity ringdown spectroscopy, Aerosol Sci. Technol., 45, 1305-1318, doi:10.1080/02786826.2011.592745, 2011.

Lawson, R. P.: Effects of ice particles shattering on the 2D-S probe. Atmos. Meas. Tech., 4(7), 1361–1381. doi:10.5194/amt-4-1361-2011, 2011.

Liao, J., Froyd, K. D., Murphy, D. M., Keutsch, F. N., Yu, G., Wennberg, P. O., St. Clair, J. M., Crounse, J. D., Wisthaler, A., Mikoviny, T., Jimenez, J. L., Campuzano-Jost, P., Day, D. A., Hu, W., Ryerson, T. B., Pollack, I. B., Peischl, J., Anderson, B. E., Ziemba, L. D., Blake, D. R., Meinardi, S., and Diskin, G.: Airborne measurements of organosulfates over the continental U.S, J. Geophys. Res. D: Atmos., 120, 2990–3005, doi:10.1002/2014JD022378, 2015.

McNaughton, C. S., Clarke, A. D., Howell, S. G., Pinkerton, M., Anderson, B., Thornhill, L., Hudgins, C., Winstead, E., Dibb, J. E., Scheuer, E., and Maring, H.: Results from the DC-8 Inlet Characterization Experiment (DICE): Airborne versus surface sampling of mineral dust and sea salt aerosols, Aerosol Sci. Technol., 41, 136–159, doi:10.1080/02786820601118406, 2007.

Moore, R. H., Wiggins, E. B., Ahern, A. T., Zimmerman, S., Montgomery, L., Campuzano Jost, P., Robinson, C. E., Ziemba, L. D., Winstead, E. L., Anderson, B. E., Brock, C. A., Brown, M. D., Chen, G., Crosbie, E. C., Guo, H., Jimenez, J. L., Jordan, C. E., Lyu, M., Nault, B. A., Rothfuss, N. E., Sanchez, K. J., Schueneman, M., Shingler, T. J., Shook, M. A., Thornhill, K. L., Wagner, N. L., and Wang, J.: Sizing response of the Ultra-High Sensitivity Aerosol Spectrometer (UHSAS) and Laser Aerosol Spectrometer (LAS) to changes in submicron aerosol composition and refractive index, Atmos. Meas. Tech., 14, 4517–4542, doi.org:10.5194/amt-14-4517-2021, 2021.

Murphy, D. M., Cziczo, D. J., Hudson, P. K., Thomson, D. S., Wilson, J. C., Kojima, T., and Buseck, P. R.: Particle generation and resuspension in aircraft inlets when flying in clouds, Aerosol Sci. Technol., 38, 401–409, doi:10.1080/02786820490443094, 2004.

Nault, B. A., Garland, C., Pusede, S. E., Wooldridge, P. J., Ullmann, K., Hall, S. R., and Cohen, R. C.: Measurements of $CH_3O_2NO_2$ in the upper troposphere, Atmos. Meas. Tech., 8, 987–997, doi:10.5194/amt-8-987-2015, 2015.

Nault, B. A., Campuzano-Jost, P., Day, D. A., Guo, H., Jo, D. S., Handschy, A. V., Pagonis, D., Schroder, J. C., Schueneman, M. K., Cubison, M. J., Dibb, J. E., Hodzic, A., Hu, W., Palm, B. B., and Jimenez, J. L.: Interferences with aerosol acidity quantification due to gas-phase ammonia uptake onto acidic sulfate filter samples, Atmos. Meas. Tech., 13, 6193–6213, doi:10.5194/amt-13-6193-2020, 2020.

Pollack, I. B., Lerner, B. M., and Ryerson, T. B.: Evaluation of ultraviolet light-emitting diodes for detection of atmospheric NO_2 by photolysis - chemiluminescence, J. Atmos. Chem., 65, 111–125, doi:10.1007/s10874-011-9184-3, 2011.

Ryerson, T. B., Williams, E. J., and Fehsenfeld, F. C.: An efficient photolysis system for fast-response NO2 measurements, J. Geophys. Res., 105(D21), 26447–26461, doi:10.1029/2000JD900389, 2000.

Sachse, G. W., Hill, G. F., Wade, L. O., and Perry, M. G.: Fast-response, high-precision carbon monoxide sensor using a tunable diode laser absorption technique. J. Geophys. Res., 92(D2), 2071–2081. doi:10.1029/JD092iD02p02071, 1987.

Schwarz, J. P., Samset, B. H., Perring, A. E., Spackman, J. R., Gao, R. S., Stier, P., Schulz, M., Moore, F. L., Ray, E. A., and Fahey, D. W.: Global-scale seasonally resolved black carbon vertical profiles over the Pacific, Geophys. Res. Lett., 40, 5542–5547, doi:10.1002/2013GL057775, 2013.

Scheuer, E., Talbot, R. W., Dibb, J. E., Seid, G. K., and DeBell, L.: Seasonal distributions of fine aerosol sulfate in the North American Arctic basin during TOPSE, J. Geophys. Res., 108, 643, doi:10.1029/2001jd001364, 2003.

Simpson, I. J., Akagi, S. K., Barletta, B., Blake, N. J., Choi, Y., Diskin, G. S., Fried, A., Fuelberg, H. E., Meinardi, S., Rowland, F. S., Vay, S. A., Weinheimer, A. J., Wennberg, P. O., Wiebring, P., Wisthaler, A., Yang, M., Yokelson, R. J., and Blake, D. R.: Boreal forest fire emissions in fresh Canadian smoke plumes: C1-C10 volatile organic compounds (VOCs), CO_2, CO, NO_2, NO, HCN and CH_3CN, Atmos. Chem. Phys., 11, 6445–6463, doi:10.5194/acp-11-6445-2011, 2011.

Skamarock, W. C., Powers, J. G., Barth, M., Dye, J. E., Matejka, T., Bartels, D., Baumann, K., Stith, J., Parrish, D. D., Hubler, G.: Numerical simulations of the July 10 Stratospheric-Tropospheric Experiment: Radiation, Aerosols, and Ozone/Deep Convection Experiment convective system: Kinematics and transport, J. Geophys. Res., 105, 19,973-19,990, doi:10.1029/2000JD900179, 2000.

Vay, S. A., Choi, Y., Vadrevu, K. P., Blake, D. R., Tyler, S. C., Wisthaler, A., Hecobian, A., Kondo, Y., Diskin, G. S., Sachse, G. W., Woo, J.-H., Weinheimer, A. J., Burkhart, J. F., Stohl, A., and Wennberg, P. O.: Patterns of CO_2 and radiocarbon across high northern latitudes during IPY 2008, J. Geophys. Res. 116, D14301, doi:10.1029/2011JD015643, 2011.

Wagner, N. L., Brock, C. A., Angevine, W. M., Beyersdorf, A., Campuzano-Jost, P., Day, D., de Gouw, J. A., Diskin, G. S., Gordon, T. D., Graus, M. G., Holloway, J. S., Huey, G., Jimenez, J. L., Lack, D. A., Liao, J., Liu, X., Markovic, M. Z., Middlebrook, A. M., Mikoviny, T., Peischl, J., Perring, A. E., Richardson, M. S., Ryerson, T. B., Schwarz, J. P., Warneke, C., Welti, A., Wisthaler, A., Ziemba, L. D., and Murphy, D. M.: In situ vertical profiles of aerosol extinction, mass, and composition over the southeast United States during SENEX and SEAC^{4}RS: observations of a modest aerosol enhancement aloft, Atmos. Chem. Phys., 15, 7085–7102, doi:10.5194/acp-15-7085-2015, 2015.

Wang S. C. and Flagan, R. C.: Scanning Electrical Mobility Spectrometer, Aerosol Sci. Technol., 13, 230–240, doi:10.1080/02786829008959441, 1990.

Yang, Q., Easter, R. C., Campuzano-Jost, P., Jimenez, J. L., Fast, J. D., Ghan, S. J., Wang, H., Berg, L. K., Barth, M. C., Liu, Y., Shrivastava, M. B., Singh, B., Morrison, H., Fan, J., Ziegler, C. L., Bela, M., Apel, E., Diskin, G. S., Mikoviny T., and Wisthaler, A.: Aerosol transport and wet scavenging in deep convective clouds: A case study and model evaluation using a multiple passive tracer analysis approach. J. Geophys. Res., 120, 8448–8468, doi:10.1002/2015JD023647, 2015.